Comparative Dynamics of Leucine Methyl Groups in FMOC-Leucine and in a Protein Hydrophobic Core Probed by Solid-State Deuteron Nuclear Magnetic Resonance over 7−324 K Temperature Range

Liliya Vugmeyster,*,† Dmitry Ostrovsky,† Mark Moses,† Joseph J. Ford,‡ Andrew S. Lipton,‡ Gina L. Hoatson,§ and Robert L. Vold§

University of Alaska—Anchorage, Anchorage, Alaska, 99508, Pacific Northwest National Laboratory, Richland, Washington, 99354, and College of William and Mary, Williamsburg, Virginia, 23187

Received: August 30, 2010; Revised Manuscript Received: October 23, 2010

Quantitative dynamics of methyl groups in 9-fluorenylmethyloxycarbonyl-leucine (FMOC-leu) have been analyzed and compared with earlier studies of methyl dynamics in chicken villin headpiece subdomain protein (HP36) labeled at L69, a key hydrophobic core position. A combination of deuteron solid-state nuclear magnetic resonance experiments over the temperature range of 7−324 K and computational modeling indicated that while the two compounds show the same modes of motions, there are marked differences in the best-fit parameters of these motions. One of the main results is that the crossover observed in the dynamics of the methyl groups in the HP36 sample at 170 K is absent in FMOC-leu. A second crossover at around 95−88 K is present in both samples. The differences in the behavior of the two compounds suggest that some of the features of methyl dynamics reflect the complexity of the protein hydrophobic core and are not determined solely by local interactions.

Introduction

The hydrophobic core of proteins plays a major role in protein stability, folding pathways, and biological function.[1] It is a complex dynamic medium reflecting the existence of a conformational ensemble. By looking at changes in the core dynamics over a very broad temperature regime, one can characterize details of the potential that govern biologically important fluctuations at the relatively narrower physiological range of temperatures.

Deuteron solid-state nuclear magnetic resonance (NMR) has been used for decades for the assessment of dynamics of many different types of materials at a variety of sample conditions.[2−17] In this paper we use solid-state deuteron NMR techniques in conjunction with computational modeling to investigate methyl dynamics. In contrast to solution state studies,[18−22] focusing attention on the solid state not only allows investigations over a much wider temperature range but also, by virtue of orientation-dependent quadrupole interactions, permits the development and critical evaluation of detailed models that describe trajectories as well as rates of different motional processes.

We are specifically interested in characteristic features of dynamics of methyl groups buried in the hydrophobic core of proteins. These solvent-protected side chains are likely to have dynamic modes that are independent of interactions with water.[20,23,24] These features should be especially apparent below 200 K, where solvent-related modes are frozen. Indeed, neutron scattering measurements indicate that protein dynamics is dominated by methyl group rotations and is independent of hydration level between 200 and 100 K.[23,25,26]

We have previously characterized the dynamics of methyl groups in a key hydrophobic core leucine residue, L69, of chicken villin headpiece subdomain protein (HP36) using deuteron line-shape analysis and spin−lattice relaxation techniques over a very broad temperature range between 300 and 4 K.[27,28] One of the main results is the existence of two crossover points: one at 170 K, at which the dynamics of the methyl group undergo a dramatic change stemming from the changes in the methyl environment, and another around 95 K, at which the dynamics undergo an abrupt freezing. The former leads to an apparent decrease in the activation energy for methyl rotation and the latter to the apparent increase in the activation energy.

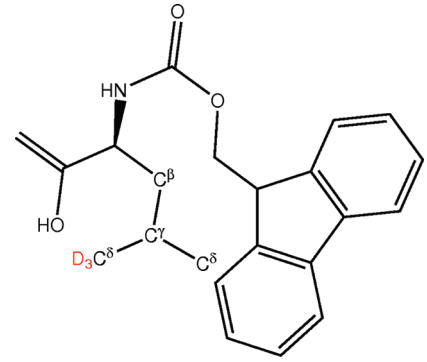

Figure 1. Structure 5,5,5-d_3 FMOC-leu with one of the labeled sites shown in red. $C^{\delta 1}$ and $C^{\delta 2}$ methyl groups are labeled in 50%/50%.

The biophysical relevance of these transitions requires further investigation. As a first step toward this goal we look at the dynamics of the methyl groups in 9-fluorenylmethyloxycarbonyl-leucine (FMOC-leu) and compare it to the results obtained for the HP36 protein. The bulky hydrophobic FMOC group (Figure 1) creates an environment similar to the hydrophobic core of a protein, yet this environment lacks the complexity inherent to the protein conformational ensemble. FMOC-leu can be thus used as a model system, which allows us to probe the influence of local structural effects, as opposed to overall

* To whom correspondence should be addressed.
† University of Alaska—Anchorage.
‡ Pacific Northwest National Laboratory.
§ College of William and Mary.

10.1021/jp1082467
Published on Web 11/15/2010

heterogeneity of the protein conformational ensemble, on the dynamics of methyl groups. In this paper we develop detailed quantitative motional models for the behavior of the FMOC-leu methyl groups and find that the crossover observed for the protein sample at 170 K is absent in FMOC-leu. We discuss in detail the differences between the motional models for the HP36 protein and FMOC-leu and their possible implications for the role of the hydrophobic core in determining the behavior of methyl groups in proteins.

Materials and Methods

Powdered 5,5,5-d_3 FMOC-Leucine was purchased from Cambridge Isotopes Laboratories (Andover, MA).

Deuteron Solid-State NMR Spectroscopy. A 17.6-T WB750 Bruker spectrometer, equipped with AVANCE I electronics and a static probe operating in the range of temperatures between 140 and 380 K, was used at the College of William and Mary. A 11.7-T WB Direct Drive Varian NMR spectrometer at Pacific Northwest National Laboratory was equipped with a magic-angle spinning (MAS) probe operating in the range of temperatures between 180 and 350 K and used with a static cryogenic helium-cooled probe[29] for temperatures below 170 K.

Line shape experiments were performed with a quadrupole echo (QE) pulse sequence with an eight-step phase cycle. The durations of 90° pulses were 3.5 μs on the 11.7-T spectrometer MAS probe and 2.0−2.7 μs on the cryogenic probe. A 2.0-μs 90° pulse was achieved with the 17.6-T spectrometer. The delay between 90° pulses was 31 μs on the 17.6-T spectrometer probe and either 30 or 40 μs on the probes used with the 11.7-T spectrometer. Data acquisition was initiated prior to the echo maximum. Time domain data were left-shifted and apodized with 100 Hz exponential broadening for temperatures above 100 K and with 1000 Hz broadening for temperatures below 100 K.

T_{1Z} (Zeeman) measurements were performed by either the inversion recovery (above 100 K) or saturation recovery (below 100 K) sequences using either quadrupolar echo[30,31] or multiple echo acquisition (QCPMG-quadrupole Carr−Purcell−Meiboom−Gill) detection schemes.[32] Briefly, QCPMG detection breaks the powder pattern spectrum into a series of spikes that follow the shape of the powder pattern. It has been recently shown that, unlike MAS, QCPMG detection does not suppress relaxation anisotropy.[33] The QCPMG detection scheme was necessary below 100 K due to either low signal intensity (for the intermediate regime described below) or long T_{1Z} values characteristic of low temperatures. Ten to fifteen QCPMG echoes were collected with 100 μs pulse spacing, corresponding to QCPMG spikes (sidebands) spaced at 10 kHz intervals. T_{1Q} (quadrupolar order) measurements were performed down to 110 K with the use of broadband Jeener−Broekaert pulse sequences and the QE detection scheme.[30,31] Six relaxation delays were typically used above 100 K and four to five below 100 K. The number of scans varied between 16 to 256 for QE detection and 8−32 for QCPMG detection.

Signal intensities for the T_{1Z} experiment were taken as the sum of intensities for the two transitions of the deuteron spins and as a difference of the intensities for T_{1Q}.[2,30] T_{1Z} relaxation times were obtained by fitting the signal intensities at selected frequencies of spectra as a function of relaxation delays to the monoexponential inversion recovery or saturation recovery functions; a monoexponential decay function was used for T_{1Q}. The only exception was the data at 87 K, for which a double-exponential decay function was used, as discussed in detail below. The errors in the measured relaxation rates, $1/T_{1Z}$ and $1/T_{1Q}$ were estimated by the asymptotic covariance matrix method.[34] In addition, for 233, 203, and 159 K temperatures at 17.6 T and for 110, 86.8, and 31 K at 11.7 T the T_{1Z} experiments were performed on two occasions and the values of T_{1Z} fell within the error limits obtained by the covariance matrix method.

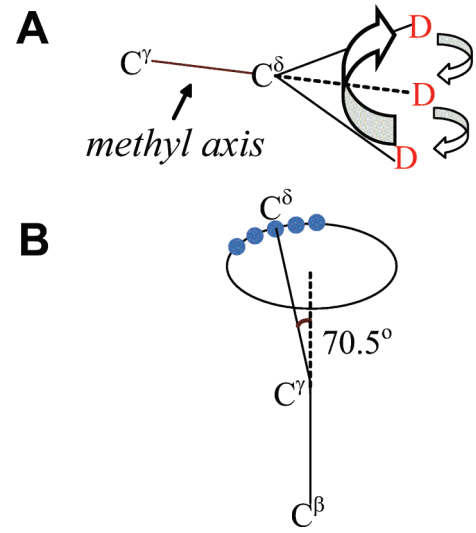

Figure 2. Schematic representation of the motional model which is used to fit the line shape data for FMOC-leu. The first mode (A) corresponds to fast 3-site hops of the methyl group; the second mode (B) corresponds to a restricted diffusion on an arc approximated by small nearest neighbor jumps of the C^γ-C^δ axis.

On the 11.7-T spectrometer, the MAS probe sample temperature was calibrated using lead nitrate with 2 kHz MAS spinning.[35] On the 17.6-T spectrometer temperature calibration was done by recording static lead nitrate line shapes[36] and using the freezing point of D_2O, 3.8 °C, as the fixed point for the calibration. The cryogenic probe on the 11.7-T spectrometer had a temperature sensor in immediate proximity to the sample area. Its reading was taken as the sample temperature.

Modeling. ***I. Deuteron Line Shapes.*** Theoretical discussions and computational approaches for computing deuteron line shapes have been presented elsewhere.[2,3,37] In this work we use the EXPRESS program discussed in detail by Vold et al.[38] Briefly, EXPRESS simulates line shapes and obtains orientation-dependent relaxation times for a number of NMR experiments by directly integrating the stochastic Liouville equation for the spin density matrix. Internal crystallite motion is represented in the Liouville equation as a matrix of Markovian jump rates between a number of sites describing possible orientations of the deuteron quadrupolar tensor principal axis system (PAS) with respect to the crystal fixed frame. EXPRESS then integrates a simulated FID signal over all possible orientations of crystallites in the laboratory frame by a tiling algorithm. The input of EXPRESS includes user-defined matrices of jump rates K_{ij}, PAS tensor orientations for each jump site, and populations for each site. Different motional modes are input with respect to different, easy to visualize nested coordinate frames with separate input parameters. EXPRESS then computes and displays an equivalent one-frame representation which is used in further computations.

Data reported here for 5,5,5-d_3 FMOC-leu were fit to a two-mode motional model (Figure 2). The first mode of motion corresponds to 3-site hops of the methyl deuterons with the rate matrix K_{ij}^{methyl}, and the second mode approximates diffusion of the C^γ-C^δ axis on a restricted arc by nearest neighbor, small angle jumps defined by a banded rate matrix K_{ij}^{arc}. The 3-site

hop motion is nested in the arc motion such that for each position of the C^{γ}-C^{δ} axis along the arc there are three possible orientations of the $C^{\delta}D_3$ group. For simplicity, the 3-fold hop rate is assumed to be independent of the instantaneous position of the C^{γ}-C^{δ} axis along the arc.

For line shape simulations in the temperature range corresponding to fast motional regime, $k^{\text{methyl}} \gg C_q \cong e^2qQ/h$, the 3-site hops of the CD_3 group are fast enough to produce a single effective axially symmetric quadrupolar tensor (directed along the C^{γ}-C^{δ} axis) with an effective quadrupolar constant of $^1/_3C_q$ if one assumes exact tetrahedral geometry. This approximation allows us to perform less computationally demanding simulations that use only the second frame instead of including both frames explicitly.

In the second frame the C^{γ}-C^{δ} axis moves on the arc of a cone with the apex angle of 141°, as defined by the tetrahedral geometry. We assume without loss of generality that the C^{γ}-C^{δ} axis has a preferred direction in the crystal-fixed frame corresponding to $\varphi = 0$, where φ is the azimuthal angle in a spherical coordinate system associated with the C^{γ} atom and the C^{β}-C^{γ} bond lies on the polar axis. The arc itself is represented by several sites with values of φ incremented in $\Delta\varphi = 5°$ steps. For example, a 50° arc is given by eleven sites with $\varphi = -25°$ to $\varphi = +25°$. The effective diffusion coefficient D is given by

$$D = \Delta\varphi^2 k^{\text{arc}} \tag{1}$$

where $k^{\text{arc}} = K^{\text{arc}}_{i,i+1} = K^{\text{arc}}_{i+1,i}$ is the jump rate between two neighboring sites in the arc frame. Only nearest-neighbor jumps are allowed. A similar approach has been used by Meints et al.[15] to describe local motions in solid DNAs. We note here that simulation of the HP36 protein line shapes required an introduction of the third frame representing jumps between differently populated conformations; this additional mode of motion is not necessary to describe the line shapes of FMOC-leu. However, these jumps do make a contribution to the relaxation data.

With the help of EXPRESS, we generated libraries of spectra using ranges of arc lengths and diffusion coefficients which gave spectral shapes visually similar to experimental data. In order to select the best parameters to fit the line shapes we minimized the following function

$$\tilde{\chi}^2 = \left(\frac{\Delta h}{h^{\text{exp}}}\right)^2 + \left(\frac{\Delta s}{s^{\text{exp}}}\right)^2 + \left(\frac{\Delta m}{m^{\text{exp}}}\right)^2 + \left(\frac{\Delta w}{w^{\text{exp}}}\right)^2 \tag{2}$$

where Δh, Δs, Δm, and Δw are differences between simulated and experimental values for the distances between horns, distances between shoulders, the ratio of intensities at the 0 kHz frequency and at the horns frequencies, and the widths of the horns measured at half height; h^{exp}, s^{exp}, m^{exp}, and w^{exp} are the experimental values of these parameters.

II. Relaxation Data. Zeeman T_{1Z} and quadrupolar order T_{1Q} relaxation rates are given by[3,4]

$$\begin{aligned}\frac{1}{T_{1Z}} &= \frac{3\pi^2}{2}C_q^2(J_1(\omega_0) + 4J_2(2\omega_0))\\ \frac{1}{T_{1Q}} &= \frac{9\pi^2}{2}C_q^2 J_1(\omega_0)\end{aligned} \tag{3}$$

where ω_0 is the Larmor frequency, J_1 and J_2 are spectral density functions, and C_q refers to the quadrupole coupling constant (units are Hz) in the absence of motion. J_1 and J_2 are dependent on time scales and types of underlying motional processes as well as on crystallite orientations. The dependence on the crystallite orientation is unique for each motional model and thus the anisotropies in the relaxation rates can be useful in discriminating among several motional models. Spectral density functions can be obtained analytically for several simple models of motion.[37] However, motional models with multiple modes usually require computer simulations.

A two-conformer model, described in detail in the Results and Discussion section, was used to fit the relaxation data between 324 and 65 K. Let r_1 and r_2 be the relaxation rates for the two conformers in the absence of exchange, p_1 and p_2 the populations of the two conformers ($p_1 + p_2 = 1$), and k_{ex} the sum of the forward and backward exchange rate constants between the conformers. Then the longitudinal component of magnetization in the two conformers can be described by the McConnell equations[39]

$$\begin{aligned}\frac{d\Delta M_1}{dt} &= -r_1\Delta M_1 - p_2k_{\text{ex}}\Delta M_1 + p_1k_{\text{ex}}\Delta M_2\\ \frac{d\Delta M_2}{dt} &= -r_2\Delta M_2 - p_1k_{\text{ex}}\Delta M_2 + p_2k_{\text{ex}}\Delta M_1\end{aligned} \tag{4}$$

where $\Delta M_{1,2}(t)$ is the difference between instantaneous magnetization of the spins in the two conformers and their respective equilibrium magnetizations. These equations are applicable if the exchange process does not contribute directly to the relaxation but only mixes relaxation processes in the two conformers. The inequality $k_{\text{ex}} \ll k^{\text{methyl}}\omega_0^2/((k^{\text{methyl}})^2 + \omega_0^2)$ ensures that the relaxation rate due to the exchange process is much smaller than the relaxation rates due to the 3-site hops in either of the conformers and, thus, is sufficient for the applicability of eq 4. We note in passing that this situation is *not* included in the current version of EXPRESS. The difference of the time-dependent magnetization from its equilibrium value $\Delta M(t) = \Delta M_1(t) + \Delta M_2(t)$ is given by the solution of eqs 4, $\Delta M(t) = (A_1e^{-\lambda_1 t} + A_2e^{-\lambda_2 t})\Delta M(0)$, where

$$\lambda_{1,2} = \frac{1}{2}(r_1 + r_2 + k_{ex} \pm \sqrt{(r_1 - r_2)^2 - 2k_{\text{ex}}(r_1 - r_2)(p_1 - p_2) + k_{\text{ex}}^2}) \tag{5}$$

and

$$A_{1,2} = \frac{1}{2}\left(1 \pm \frac{(r_1 - r_2)(p_1 - p_2) - k_{\text{ex}}}{\sqrt{(r_1 - r_2)^2 - 2k_{\text{ex}}(r_1 - r_2)(p_1 - p_2) + k_{\text{ex}}^2}}\right) \tag{6}$$

in which we assumed that the initial magnetizations $\Delta M_1(0)$ and $\Delta M_2(0)$ are proportional to the equilibrium populations p_1 and p_2, respectively. Thus, in general, the two-conformer model implies a double-exponential decay. We consider two qualitatively different limits that are important for selection of a correct model.

(1) $|r_1 - r_2| \ll k_{\text{ex}}$. In this limit $\lambda_1 \approx k_{\text{ex}} + p_2r_1 + p_1r_2$, $\lambda_2 \approx p_1r_1 + p_2r_2$, and the amplitudes are $A_1 \approx 2p_1p_2(r_1 - r_2)^2/k_{\text{ex}}^2 \ll 1$ and $A_2 \approx 1$. Thus, the component decaying with the rate λ_1 is always much smaller than the component decaying with the rate λ_2, and

experimentally one observes an almost monoexponential decay with the relaxation rate of $p_1r_1 + p_2r_2$.

(2) $|r_1 - r_2| \gg k_{ex}$. In this limit $\lambda_1 \approx r_1 + p_2k_{ex}$ and $\lambda_2 \approx r_2 + p_1k_{ex}$ with $A_1 \approx p_1$ and $A_2 \approx p_2$, in which we assumed $r_1 > r_2$. This is the limit of two slowly exchanging conformers. If p_1 and p_2 are comparable (otherwise, the model will be indistinguishable from the single conformer model), one will observe a double exponential decay in the T_{1Z} experiment. The conditions $|r_1 - r_2| \gg k_{ex}$ and $r_1 > r_2$ imply that $r_1 \gg k_{ex}$. The relationship between r_2 and k_{ex} is not fixed in this limit. When $r_2 \gg p_1k_{ex}$ one has a limit of two almost independent conformers, which leads to double-exponential relaxation curves with the rates determined by the relaxation in each conformer. If, on the other hand, $r_2 \ll p_1k_{ex}$ then $\lambda_2 \approx p_1k_{ex}$. Note that in the latter limit neither of the relaxation rates depends on r_2.

For temperatures in the 324−90 K range the fast exchange approximation corresponding to the $|r_1 - r_2| \ll k_{ex}$ limit was adequate. Each conformer followed the two-mode model described in the Deuteron Line Shapes section, with the temperature-dependence of the 3-site hop motion governed by the Arrhenius Law $k^{methyl} = k_0 \exp(-E_a/RT)$ and the parameters of the arc motion fixed from the line shape analysis. There are five parameters in this model: activation energies E_a and prefactors k_0 for each conformer, and the energy difference between the two conformers. As explained in the Results and Discussion section, the model was reduced to three fitting parameters only: one value of the activation energy that was the same for both conformers and two different values for the prefactors. The ratio of populations of the two conformers was fixed at 1:1 for all temperatures.

For each temperature a library of relaxation rates was created as a function of k^{methyl} and then the predicted relaxation rate was obtained as a weighted-average rate for the two conformers. Finally, the predicted rates were compared with the experimental values, and best-fit parameters were obtained through χ^2 minimization. The errors in fitted parameters were estimated by the covariance matrix method.[34]

As explained in the Results and Discussion section, for the temperature range between 90 and 65 K the slow exchange approximation corresponding to the $|r_1 - r_2| \gg k_{ex}$ limit gives an adequate description of the experimental data. For such low temperatures, arc motions can be completely ignored and the selection of the model parameters to fit the experimental data is straightforward.

III. Effects of Tunneling on Deuteron Relaxation. At low temperatures quantum mechanical effects of tunneling can play a major role in the description of both line shapes and relaxation of deuterated methyl groups.[40−42] The onset of tunneling is expected to occur below 90−60 K, with the exact temperature determined by the details of the hindering 3-fold potential.

The effect of tunneling on the spectral densities contributing to the relaxation times according to eq 3 can be described by[40]

$$J_1(\omega_0) \rightarrow \frac{1}{3}(J_1(\omega_0) + J_1(\omega_0 + \omega_t) + J_1(\omega_0 - \omega_t))$$
$$J_2(2\omega_0) \rightarrow \frac{1}{3}(J_2(2\omega_0) + J_2(2\omega_0 + \omega_t) + J_2(2\omega_0 - \omega_t)) \quad (7)$$

where $\omega_t(T)$ is the temperature-dependent tunneling frequency. The last terms in these equations demonstrate the possibility of the resonance conditions for $\omega_t(T) = \omega_0$ or $\omega_t(T) = 2\omega_0$, such that one observes maxima in the relaxation rate. Note that the prominence of the maximum depends strongly on the correlation time of motions in the 3-fold potential. The temperature dependence of the relaxation times in this limit is governed primarily by the effective energy splitting between torsional levels.

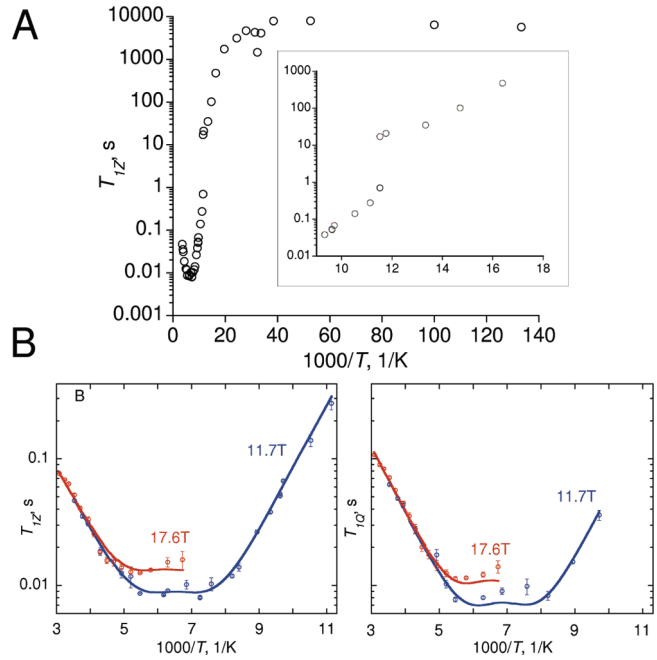

Figure 3. Semilog plots of deuteron relaxation times at frequencies of maximum intensity versus 1000/T for FMOC-leu. (A) Entire temperate range between 324 and 7.5 K is shown for data at 11.7 T. The insert displays an expanded plot for the 95−65 K range. Two values are shown for 86.8 K (see text). (B) T_{1Z} and T_{1Q} relaxation times at 17.6 T (red circles) and 11.7 T (blue circles) for 324−90 K temperature range. Simulated data (solid lines) were generated according to the two-rotamer model described in the text.

Results and Discussion

The deuteron label in FMOC-leu is equally distributed between the two C^{δ} positions. Thus, all of our line shape and relaxation measurements have contributions from both positions. MAS experiments at room temperature did not resolve any differences in chemical shift between the two positions. Moreover, there was no indication of nonequivalent sites in any of QCPMG line shapes or relaxation rates. Thus, the two positions can be treated as identical. The same conclusion has been reached for the protein sample.

A plot of T_{1Z} vs $1/T$ data at 500 MHz (Figure 3) over the entire temperature range between 324 and 7.5 K reveals three types of behavior: in the 324−90 K range the curve is roughly consistent with an Arrhenius law for fast methyl rotation, over the range 90−60 K T_{1Z} continues to increase but there is a jump in T_{1Z} values, and for temperatures below 50 K T_{1Z} values level off accompanied by a resonance feature at around 31 K. We will analyze the results for these three different regimes separately.

Temperature Range 324−90 K. In this temperature regime we obtained the data at two fields: 11.7 and 17.6 T. Also, in addition to the T_{1Z} (Zeeman) relaxation times, we measured T_{1Q} (quadrupolar order) relaxation times. Combined with line shape data, this wealth of information allows us to construct a precise motional model for the motion of the $-CD_3$ groups.

I. Line Shapes at High Temperatures Can Be Modeled by Diffusive Motion along a Restricted Arc. Figure 4 presents experimental line shapes obtained with the quadrupolar echo

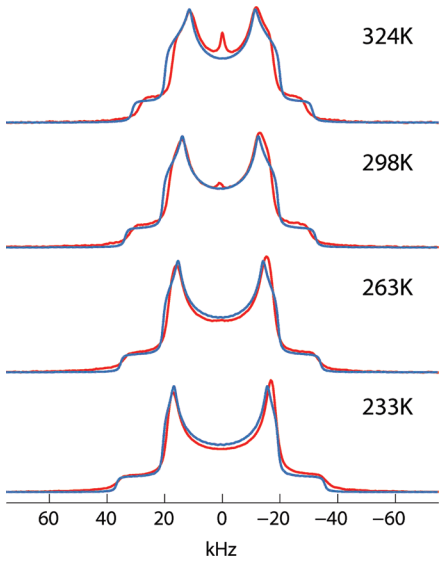

Figure 4. Experimental (red) and simulated (blue) quadrupolar echo line shapes of FMOC-leu for the fast motional limit with respect to the 3-site hops rate constants.

pulse sequence. The overall line shapes at high temperatures are characteristic of fast methyl group rotation for which the rate of 3-site jumps is much faster than the quadrupolar coupling constant C_q and the width of the powder pattern spectrum is given by $\sim^1/_3 C_q$. It is clear, however, that at higher temperatures additional slower motions are present on the millisecond−microsecond time scale. These additional motions lead to further narrowing of the powder pattern, accompanied by slanted shoulders and a build-up of extra intensity in the middle of the spectra. Thus, the presence of a small asymmetry parameter is clearly visible. Interestingly, this asymmetry is not present in the line shapes of L-[δd_3]-leucine[9] and D,L-[d_{10}]-leucine.[6]

The 3-site jump mode can not account for the asymmetry (Supporting Information). Motional models consisting of either axially symmetric rotation about the methyl axis or small-angle symmetric jumps of the methyl axis are also incapable of accounting for the observed asymmetry. A plot of intensity taken at the maximum of the echo vs temperature (Supporting Information) gives the temperature dependence consistent with the build-up of magnetization according to the Boltzmann distribution. This result excludes a model with large-angle jumps, which would show a characteristic minimum in the intensity versus temperature plots.

A simple model that is consistent with the molecular geometry and that does introduce a small asymmetry is diffusion on a restricted arc (Figure 2).[27] Spectra simulated according to the model that combines 3-site jumps and diffusion on a restricted arc are shown in Figure 4. The arc length varies from 80° at 324 K to about 45° at 213 K. Its temperature dependence is roughly linear with the following parameters: the slope of 0.34°/K and the intercept of −29°. Below 213 K the line shapes are consistent with the arc length leveling off to about 35° and the diffusion coefficient following the Arrhenius law with $D_0 = 4.8 \times 10^6$ rad^2/s and $E_a^s = 9.4$ kJ/mol. The temperature dependence of the diffusion coefficient and arc length is shown in the Supporting Information. The central peak at high temperatures is due to trace water (HOD) signal.

How do these line shape results compare to the one obtained for the HP36 protein labeled at the methyl group of L69? In the protein sample restricted diffusion on the arc is apparent as well. The diffusion coefficient is temperature dependent, but the arc length remains at a constant value of 35° for all temperatures. Thus, the amplitude of the diffusive motion is much larger in FMOC-leu due to the dominance of a restoring potential, while in the protein sample steric interactions restrict the motions on the arc.

Interestingly, the line shapes for the protein sample displayed an additional mode of motion corresponding to large-angle rotameric jumps. This mode is not reflected in the line shapes for FMOC-leu. We will see in the following section that the rotameric jumps do make a contribution to the relaxation data. The fact that this mode is not visible from the line shapes indicates that the rate of the jumps is much slower than the quadrupolar coupling constant.

II. Relaxation Data Fitted by the Presence of Two Rotamers. Relaxation data probe motions on a time scale close to the Larmor frequency. Fast 3-site hops of C^δ methyl groups in leucine side-chains occur on pico- to sub-nanosecond time scales in this temperature regime and are the main contribution to the relaxation rates. T_{1Z} and T_{1Q} relaxation times at horn positions in the temperature regime between 324 and 90 K are presented in Figure 3B. It is immediately apparent that the 3-site hop mechanism with a *single* activation energy can not describe the data because the minima would be roughly 40−50% smaller in magnitude and much sharper. We thus need a more involved model to account for the observed trend. We explored several additions to a simple 3-site hop model to account for the observed temperature dependence of the relaxation times, including distribution of activation energies, distribution of prefactors, the presence of two independent noninteracting conformations, and phase transitions in which the parameters of the Arrhenius law change abruptly. None of these features nor their combinations succeeded in explaining the trend.

The following model is successful in explaining the temperature dependence of the relaxation times: in addition to the fast 3-site hops and slow diffusion on a restricted arc, the side chain undergoes a chemical exchange between two conformations with the same values of activation energies but somewhat different prefactors. The slow motion along the restricted arc gives a small additional contribution to the relaxation rates up to 5%. The parameters of the arc motion are fixed from the line shape data as described above. In principle, there are five fitting parameters in this model: two values of the prefactors, two values of the activation energies, and the energy difference between the two conformations. Having two different values for the activation energies or a nonzero value of the energy difference between the two states have not yielded any statistically significant improvement, and we have therefore used a three parameter fit with a fixed 1:1 ratio of the two conformers at all temperatures.

Relaxation time anisotropy profiles can be a useful means of discriminating between motional models.[3,37] The presence of the anisotropy itself supports the 3-site hops model as opposed to rotational diffusion of the methyl groups in agreement with earlier works.[43] The extent of anisotropy in the experimental data is somewhat smaller than the one predicted from the 3-site hops mode alone. The addition of the slow arc motion reduces the extent of anisotropy in the simulated rates. Simulations according to the two-conformer model, including the restricted diffusion mode, yielded relaxation anisotropy profiles consistent with the experiment (Supporting Information).

All experimental relaxation data are single-exponential within the precision of the measurement. Thus, the exchange between the two states has to be on a time scale fast enough to average

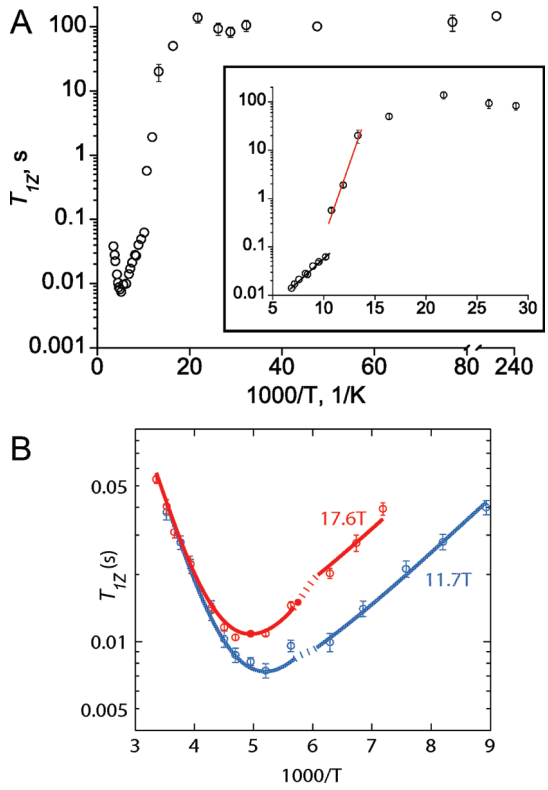

Figure 5. Semilog plots of deuteron T_{1Z} relaxation times versus 1000/T for L69 in HP36 protein, as reported in previous studies.[27,28] (A) entire temperate range between 298 and 4 K is shown for data at 11.7 T. The insert displays an expanded plot for the 140 to 50 K range. Solid lines represent the best Arrhenius fit for either 160−98 K temperature range (black) or 98−75 K temperature range (red). (B) Existence of the crossover at 170 K is demonstrated by showing 300−112 K temperature range for the relaxation times at horn positions at 17.6 T (red circles) and 11.7 T (blue circles) along with the simulated data (solid lines). Dotted line indicates the crossover region.

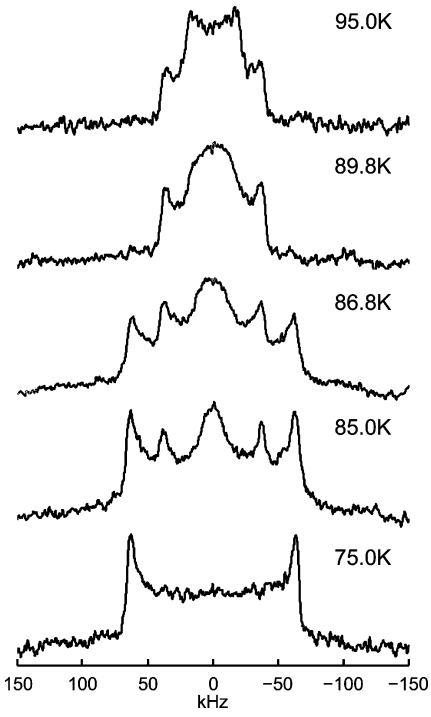

Figure 6. Experimental quadrupolar echo line shapes of FMOC-leu for the intermediate (95−85 K) and slow (75 K) motional regimes.

the relaxation rates of the two conformations but slow enough to avoid contributions to the line shapes. Therefore, the limit of fast exchange $|r_1 - r_2| \ll k_{ex}$ can be used to model the relaxation rates. The two conformations likely represent the two most populated rotamers of leucine side chains out of nine possible configurations. These two rotamers correspond to the following values of the dihedral angles: $\chi_1 = 300°$, $\chi_2 = 180°$ and $\chi_1 = 180°$, $\chi_2 = 60°$.[44] Simulated relaxation times at the horn positions are shown by solid lines in Figure 3B. The fitted values of the parameters are: the activation energy 9.7 ± 0.2 kJ/mol, and the Arrhenius prefactors for the two conformations are$1.7 \times 10^{11} \pm 0.1 \times 10^{11}$ and $1.5 \times 10^{12} \pm 0.1 \times 10^{12}$ s^{-1}.

Comparison with the relaxation data for HP36 protein is quite striking: rotameric jumps are not prominent in the relaxation data for the protein due to the dominant population of one major conformer. Instead, the relaxation data for the protein are dominated by a distribution of the activation energies at high temperatures which collapses to a single much smaller value at around 170 K (Figure 5). This crossover behavior is absent in FMOC-leu, indicating that the complexity of a protein environment is a necessary feature of the phenomenon.

Temperature Range 90−60 K Reveals the Presence of a Structural Transition. Below we present several pieces of experimental evidence that convince us that around 90 K there is a change in the behavior of the methyl groups, which is likely to arise from a structural transition in FMOC-leu.

The first piece of evidence stems from a careful examination of the line shape and relaxation data at 86.8 K. The second piece of evidence arises from the analysis of the Arrhenius plot of the relaxation times in this temperature range (Figure 3A).

Unlike the intermediate regime spectra at higher temperatures (Figure 6), the line shape at 86.8 K shows a distinct presence of "horns" at about ±60 kHz, which are indicative of 3-site hops in the slow regime. The maximum rate of the hops that give rise to the horns is about 7000 s^{-1}, which is much smaller than the one predicted from extrapolation of the Arrhenius law for either of the conformers; the extrapolated rates are 2.3×10^5 s^{-1} and 2.1×10^6 s^{-1}. Overall, the spectrum can be characterized as having a feature characteristic of methyl rotation in the slow regime ($k^{methyl} \ll C_q$), which is responsible for the appearance of horns at approximately ±60 kHz, and another feature characteristic of rotation in the intermediate regime ($k^{methyl} \approx C_q$), which gives rise to the distinct spectral pattern between −40 and 40 kHz. The T_{1Z} data show that while for the ±60 kHz peaks one has reasonably good monoexponential decay curves corresponding to $T_{1Z} \approx 17$ s the T_{1Z} decay curves at ±40 and 0 kHz show very clear nonmonoexponential behavior (Supporting Information). A double-exponential fit gives the relaxation times of 17 ± 2 and 0.7 ± 0.1 s.

For the spectral positions of ±60 kHz at 86.8 K, as well as for all frequencies at 85 and 75 K, the experimental relaxation times are much longer than those predicted by the Arrhenius law with the parameters of the high temperature regime for either conformer (Supporting Information) They are also much shorter than the relaxation times for a simple 3-site hops motion compatible with the presence of a full width Pake-pattern component in the spectrum. Thus, we conclude that at these temperatures the limit of fast exchange breaks down.

However, the reverse limit, $|r_1 - r_2| \gg k_{ex}$, can explain the data. Indeed, if an even more stringent condition $r_1 \gg k_{ex} \gg r_2$ is assumed then the relaxation rate corresponding to the full-width (slow) component of the spectrum is determined by k_{ex} rather than by r_2. We can thus reconcile the presence of the

full-width component with its relatively large apparent relaxation rate. The relaxation of the middle part of the spectrum (i.e., from −40 to +40 kHz) is determined by r_1. If we assume that both conformers have equal weights, i.e., $p_1 = p_2 = 0.5$ for all temperatures, which gave the best fit for the higher temperature regime and is consistent with a detailed analysis of the data at 86.8 K, then the experimental data allow us to fix k_{ex} at 0.12, 0.095, 0.057, 0.020, and 0.0042 s^{-1} for 86.8, 85, 75, 68, and 61 K, respectively, as well as r_1 at 1.3 s^{-1} for 86.8 K.

At 75 K the spectrum (Figure 6) almost reaches the slow regime, and the relaxation data are single-exponential at all frequencies. This may be due to the faster conformer being deep in the intermediate regime, at which the intensity drops dramatically compared to the slower conformer. At 68 and 61 K the spectra display full-width Pake patterns and the relaxation is single-exponential. Finally, we note that T_{1Z} values in the 86.8−61 K temperature interval roughly follow the Arrhenius law, which may be a reflection of the Arrhenius law for k_{ex}.

The comparison of results at 89.8 and 86.8 K shows that the methyl environment undergoes a dramatic change between these two temperatures. Indeed, at 89.8 K the model of two rapidly interconverting conformers which follow the Arrhenius law with the parameters fixed by the high temperature regime gives predictions that are in good agreement with the experimental data. If the same approach were also valid for 86.8 K, one would expect the following values of the relaxation rates for the two conformers for the validity of the model: $r_1 = 4.1$ s^{-1} and $r_2 = 0.38$ s^{-1}. However, the parameters obtained above for the model of slowly interconverting conformers are dramatically different; r_1 is more than 3 times lower, r_2 is at least 30 times lower, and k_{ex} is smaller by at least 2 orders of magnitude compared to the predictions of the high temperature model extrapolated to this temperature.

This implies that in the narrow temperature range around 89−88 K FMOC-leu powder undergoes a structural change which affects the local potentials of the methyl groups. Since in the 87−61 K temperature range the experimental relaxation rates are dominated by the exchange rate of the two conformers, we can not determine the changes in the activation energy and, hence, can not characterize the changes in the local potential in detail.

We have previously shown that the hydrophobic core methyl groups of L69 in HP36 protein undergo a transition around 95 K, as evidenced by a distinct increase in the apparent activation energy. Thus, it appears that the methyls in both FMOC-leu and L69 in HP36 experience a change in their environment which affects the relaxation rates. However, we can not determine whether the nature of these changes is the same in the two samples.

Temperature Range 60−7.5 K Is Dominated by Deuteron Tunneling. Below 60 K the onset of tunneling is evident from the relaxation data (Figure 3A). At about 50 K the Arrhenius curve becomes concave, and the rates eventually level out completely at approximately 25 K.

A prominent low-temperature feature is the appearance of the T_1 minimum (R_1 maximum) at 31 K. According to eq 7 this feature is expected when $\omega_t(T) = \omega_0$ or $\omega_t(T) = 2\omega_0$. Thus, the presence of the minimum fixes the tunneling frequency at either 76 or 152 MHz at 31 K. Field-dependent relaxation data would be helpful in this situation to discriminate between the two values of the tunneling frequency. No minimum has been observed for the HP36 sample. However, no conclusion can be drawn on this basis because the data step size of 1 K would be necessary for a careful search for the presence of the minimum.

The relaxation times in FMOC-leu level off to a value of about 6500 s, implying a very inefficient relaxation mechanism. Interestingly, the relaxation times for L69 in HP36 also level out at low temperatures, albeit to a significantly smaller value of about 150 s. As discussed in the "Materials and Methods" section, at these low temperatures the energy difference between torsional states, mainly the ground and first excited states, govern the relaxation rates outside the region of the resonance peak. Thus, in both FMOC-leu and L69 in HP36 the energy differences between the torsional states are small, but the resulting relaxation times are much smaller in the protein.

Conclusions

We have utilized solid-state deuteron NMR to look at the dynamics of methyl groups in FMOC-leu and compare it to the dynamics of the hydrophobic core of HP36 protein labeled at a key methyl group of L69. Studies over a very broad temperature range between 324 and 7.5 K yielded very detailed motional models. Similar multimodal models can be applied to both compounds. The modes of motion are 3-site hops of the methyl group, diffusion on a restricted arc of the methyl axis itself, and large angle rotameric jumps. However, there are marked differences in the parameters of these motions. There is one dominant rotamer in the protein sample, whereas FMOC-leu has two equally populated rotamers; the time scales of the rotameric jumps are much faster in the protein than in FMOC-leu; the arc motion has a smaller, temperature-independent amplitude in the protein, while in FMOC-leu the length of the arc is larger and strongly depends on temperature. The constraints obtained by the combination of line shape and relaxation data are very stringent and do not allow for much ambiguity in the choice of the models.

Relaxation behavior in HP36 at higher temperatures is dominated by a distribution of the activation energies for the 3-site hops which collapses to a single much smaller value at around 170 K. In contrast, for FMOC-leu the activation energy has a single, well-defined value throughout the 324−90 K temperature range. Thus, the complexity of the hydrophobic core environment appears to be necessary for the existence of such a crossover.

Upon lowering the temperature to about 95 K, L69 in HP36 showed the freezing of methyl dynamics as manifested by a sharp increase in the apparent activation energy value. The detailed analysis of relaxation times in FMOC-leu, which show a distinct jump around 89−88 K, as well as the line shapes analysis in the intermediate regime, suggest that FMOC-leu undergoes a structural change which affects the local potentials of the methyl groups. However, in the temperature range of 89−61 K the relaxation rates are dominated by the exchange rate of the two rotamers and not by the rate constants of the 3-site hops, and hence the activation energies for methyl hops could not be determined. Therefore, it is difficult to judge whether the structural change in the FMOC-leu has the same nature as the freezing of methyl group dynamics in the protein.

Finally, at very low temperatures below 50 K the onset of deuteron tunneling is apparent in the relaxation behavior of both compounds. We were able to observe a tunneling T_1 minimum for FMOC-leu at about 31 K. The relaxation times eventually level out to a constant value, indicating that the energy differences between the torsional states are small. However, this limiting value of the relaxation time is 40 times larger in FMOC-leu compared to the one in the HP36 sample.

The comparison between the behavior of a key hydrophobic core residue in HP36 protein and FMOC-leu molecule, which mimics the hydrophobic core environment yet lacks the complexity of the protein core, is very instructive. It shows that while there are a number of similarities in the methyl group dynamics of the two compounds some of the features are likely to require the complexity of the protein and are not determined solely by local interactions.

Acknowledgment. L.V. acknowledges Cottrell College Science Award from Research Corporation for Science Advancement, Research Opportunity Award from NSF-CHE-0713819 Grant to R.L.V, University of Alaska funds 104110-11970 and 11470, and Environment and Natural Resources Institute, University of Alaska at Anchorage. Part of this research was performed using EMSL, a national scientific user facility sponsored by the Department of Energy's Office of Biological and Environmental Research located at Pacific Northwest National Laboratory. NMR data at 17.6 T were collected at the College of William and Mary NMR laboratory, which is supported by NSF Grant No. CHE-0713819 to the College of William and Mary on behalf of R.L.V. and G.L.H. We are grateful to Jesse Sears and Sarah Burton for technical assistance.

Supporting Information Available: Figures depicting the comparison of the experimental line-shape at 298 K with the simulated spectrum obtained using exclusively the 3-site jump mode, intensity at echo maximum of QE spectra vs temperature, arc length and diffusion coefficient as a function of temperature, relaxation anisotropy profiles at 298 K, intensity vs time curve for T_{1Z} at zero frequency at 86.8 K, and detailed analysis of T_{1Z} data for the 95−65 K range. This material is available free of charge via the Internet at http://pubs.acs.org.

References and Notes

(1) Creighton, T. E. *Proteins: structures and molecular properties*; Freeman and Company: New York, 1993.

(2) Vold, R. R., Deuterium NMR studies of dynamics in solids and liquid crystals. In *Nuclear Magnetic Resonance Probes of Molecular Dynamics*; Tycko, R., Ed.; Kluwer Academic Publishers: Dordrecht, 1994; pp 27−112.

(3) Vold, R. L.; Vold, R. R. Deuterium Relaxation in Molecular Solids. In *Advances in Magnetic and Optical Resonance*; Warren, W. , Ed.Academic Press: San Diego, 1991; Vol. 16, pp 85−171.

(4) Duer, M. J. *Solid-State NMR Spectroscopy.*: Blackwell Publishing Ltd: Oxford, 2004.

(5) Krushelnitsky, A.; Reichert, D. Solid-state NMR and protein dynamics. *Prog. Nucl. Magn. Reson. Spectrosc.* **2005**, *47* (1−2), 1–25.

(6) Batchelder, L. S.; Sullivan, C. E.; Jelinski, L. W.; Torchia, D. A. Characterization of leucine side-chain reorientation in collagen fibrils by solid-state H-2 NMR. *Proc. Natl. Acad. Sci. U. S. A.* **1982**, *79* (2), 386–389.

(7) Brown, M. F.; Heyn, M. P.; Job, C.; Kim, S.; Moltke, S.; Nakanishi, K.; Nevzorov, A. A.; Struts, A. V.; Salgado, G. F. J.; Wallat, I. Solid-State H-2 NMR spectroscopy of retinal proteins in aligned membranes. *Biochim. Biophys. Acta, Biomembr.* **2007**, *1768*, 2979–3000.

(8) Copie, V.; McDermott, A. E.; Beshah, K.; Williams, J. C.; Spijkerassink, M.; Gebhard, R.; Lugtenburg, J.; Herzfeld, J.; Griffin, R. G. Deuterium solid-state nuclear-magnetic-resonance studies of methyl-group dynamics in bacteriorhodopsin and retinal model compounds - evidence for a 6-S-trans chromophore in the protein. *Biochemistry* **1994**, *33* (11), 3280–3286.

(9) Keniry, M. A.; Kintanar, A.; Smith, R. L.; Gutowsky, H. S.; Oldfield, E. Nuclear magnetic-resonance studies of amino-acids and proteins - deuterium nuclear magnetic-resonance relaxation of deuteriomethyl-labeled amino-acids in crystals and in halobacterium-halobium and escherichia-coli cell-membranes. *Biochemistry* **1984**, *23* (2), 288–298.

(10) Mack, J. W.; Usha, M. G.; Long, J.; Griffin, R. G.; Wittebort, R. J. Backbone motions in a crystalline protein from field-dependent H-2-NMR relaxation and line-shape analysis. *Biopolymers* **2000**, *53* (1), 9–18.

(11) Pometun, M. S.; Chekmenev, E. Y.; Wittebort, R. J. Quantitative observation of backbone disorder in native elastin. *J. Biol. Chem.* **2004**, *279* (9), 7982–7987.

(12) Reif, B.; Xue, Y.; Agarwal, V.; Pavlova, M. S.; Hologne, M.; Diehl, A.; Ryabov, Y. E.; Skrynnikov, N. R. Protein side-chain dynamics observed by solution- and solid-state NMR: Comparative analysis of methyl H-2 relaxation data. *J. Am. Chem. Soc.* **2006**, *128* (38), 12354–12355.

(13) Tamura, A.; Matsushita, M.; Naito, A.; Kojima, S.; Miura, K. I.; Akasaka, K. Dynamics of the three methionyl side chains of Streptomyces subtilisin inhibitor. Deuterium NMR studies in solution and in the solid state. *Protein Sci.* **1996**, *5* (1), 127–139.

(14) Ying, W. W.; Irvine, S. E.; Beekman, R. A.; Siminovitch, D. J.; Smith, S. O. Deuterium NMR reveals helix packing interactions in phospholamban. *J. Am. Chem. Soc.* **2000**, *122* (45), 11125–11128.

(15) Meints, G. A.; Miller, P. A.; Pederson, K.; Shajani, Z.; Drobny, G. Solid-state nuclear magnetic resonance spectroscopy studies of furanose ring dynamics in the DNA Hhal binding site. *J. Am. Chem. Soc.* **2008**, *130* (23), 7305–7314.

(16) Olsen, G. L.; Echodu, D. C.; Shajani, Z.; Bardaro, M. F.; Varani, G.; Drobny, G. P. Solid-state deuterium NMR studies reveal mu s-ns motions in the HIV-1 Transactivation response RNA recognition site. *J. Am. Chem. Soc.* **2008**, *130* (10), 2896–2897.

(17) Weidner, T.; Breen, N. F.; Li, K.; Drobny, G.; Castner, D. G. Sum frequency generation and solid-state NMR study of the structure, orientation, and dynamics of polystyrene-adsorbed peptides. *Proc. Natl. Acad. Sci. U S A* **2010**, *107*, 13288–13293.

(18) Agarwal, V.; Xue, Y.; Reif, B.; Skrynnikov, N. R. Protein side-chain dynamics as observed by solution- and solid-state NMR spectroscopy: a similarity revealed. *J. Am. Chem. Soc.* **2008**, *130* (49), 16611–16621.

(19) Hansen, D. F.; Neudecker, P.; Vallurupalli, P.; Mulder, F. A. A.; Kay, L. E. Determination of Leu side-chain conformations in excited protein states by NMR relaxation dispersion. *J. Am. Chem. Soc.* , *132* (1), 42–+.

(20) Lee, A. L.; Wand, A. J. Microscopic origins of entropy, heat capacity and the glass transition in proteins. *Nature* **2001**, *411* (6836), 501–504.

(21) Igumenova, T. I.; Frederick, K. K.; Wand, A. J. Characterization of the fast dynamics of protein amino acid side chains using NMR relaxation in solution. *Chem. Rev.* **2006**, *106* (5), 1672–1699.

(22) Mauldin, R. V.; Lee, A. L. Nuclear magnetic resonance study of the role of M42 in the solution dynamics of Escherichia coli Dihydrofolate Reductase. *Biochemistry* , *49* (8), 1606–1615.

(23) Doster, W. The dynamical transition of proteins, concepts and misconceptions. *Eur. Biophys. J.* **2008**, *37* (5), 591–602.

(24) Bajaj, V. S.; van der Wel, P. C. A.; Griffin, R. G. Observation of a low-temperature, dynamically driven structural transition in a polypeptide by solid-state NMR Spectroscopy. *J. Am. Chem. Soc.* **2009**, *131* (1), 118–128.

(25) Roh, J. H.; Novikov, V. N.; Gregory, R. B.; Curtis, J. E.; Chowdhuri, Z.; Sokolov, A. P. Onsets of anharmonicity in protein dynamics. *Phys. Rev. Lett.* **2005**, *95* (3), 038101.

(26) Wood, K.; Tobias, D. J.; Kessler, B.; Gabel, F.; Oesterhelt, D.; Mulder, F. A. A.; Zaccai, G.; Weik, M. The Low-temperature inflection observed in neutron scattering measurements of proteins is due to methyl rotation: direct evidence using isotope labeling and molecular dynamics simulations. *J. Am. Chem. Soc.* **2010**, *132* (14), 4990–4991.

(27) Vugmeyster, L.; Ostrovsky, D.; Ford, J. J.; D., B. S.; Lipton, A. S.; Hoatson, G. L.; Vold, R. L. Probing the dynamics of a protein hydrophobic core by deuteron solid-state nuclear magnetic resonance spectroscopy. *J. Am. Chem. Soc.* **2009**, *131* (38), 13651–13658.

(28) Vugmeyster, L.; Ostrovsky, D.; Ford, J. J.; Lipton, A. S. Freezing of dynamics of a methyl group in a protein hydrophobic core at cryogenic temperatures by deuteron NMR spectroscopy. *J. Am. Chem. Soc.* **2010**, *132* (12), 4038–4039.

(29) Lipton, A. S.; Heck, R. W.; Sears, J. A.; Ellis, P. D. Low temperature solid-state NMR experiments of half-integer quadrupolar nuclides: caveats and data analysis. *J. Magn. Reson.* **2004**, *168* (1), 66–74.

(30) Hoatson, G. L. Broad-Band composite excitation sequences for creating quadrupolar order in H-2 NMR. *J. Magn. Reson.* **1991**, *94* (1), 152–159.

(31) Wimperis, S. Broad-band and narrow-band composite excitation sequences. *J. Magn. Reson.* **1990**, *86* (1), 46–59.

(32) Larsen, F. H.; Jakobsen, H. J.; Ellis, P. D.; Nielsen, N. C. High-field QCPMG-MAS NMR of half-integer quadrupolar nuclei with large quadrupole couplings. *Mol. Phys.* **1998**, *95* (6), 1185–1195.

(33) Vold, R. L.; Hoatson, G. L.; Vugmeyster, L.; Ostrovsky, D.; De Castro, P. J. Solid state deuteron relaxation time anisotropy measured with multiple echo acquisition. *Phys. Chem. Chem. Phys.* **2009**, *11* (32), 7008–7012.

(34) Shao, J. *Mathematical Statistics*; Springer: New York, 2003.

(35) Neue, G.; Dybowski, C. Determining temperature in a magic-angle spinning probe using the temperature dependence of the isotropic chemical shift of lead nitrate. *Solid State Nucl. Magn. Reson.* **1997**, *7* (4), 333–336.

(36) Beckmann, P. A.; Dybowski, C. A thermometer for nonspinning solid-state NMR spectroscopy. *J. Magn. Reson.* **2000**, *146* (2), 379–380.

(37) Torchia, D. A.; Szabo, A. Spin-Lattice Relaxation in Solids. *J. Magn. Reson.* **1982**, *49* (1), 107–121.

(38) Vold, R. L.; Hoatson, G. L. Effects of jump dynamics on solid state nuclear magnetic resonance line shapes and spin relaxation times. *J. Magn. Reson.* **2009**, *198* (1), 57–72.

(39) McConnell, H. M. Reaction rates by nuclear magnetic resonance. *J. Chem. Phys.* **1958**, *28* (3), 430–431.

(40) Diezemann, G.; Sillescu, H.; van der Putten, D. Spin-lattice relaxation rates of tunneling CD3 groups. *Z. Phys. B Con. Mat.* **1991**, *83* (2), 245–257.

(41) Heuer, A. Quantum-mechanical behavior of deuterated methyl-groups - the temperature dependences of NMR-spectra and spin-lattice relaxation-Times. *Z. Phys. B* **1992**, *88* (1), 39–51.

(42) Horsewill, A. J.; Quantum tunnelling aspects of methyl group rotation studied by, N. M. R. *Prog. Nucl. Magn. Reson. Spec.* **1999**, *35* (4), 359–389.

(43) Batchelder, L. S.; Niu, C. H.; Torchia, D. A. Methyl reorientation in polycrystalline amino-acids and peptides - a H-2 NMR spin-lattice relaxation study. *J. Am. Chem. Soc.* **1983**, *105* (8), 2228–2231.

(44) Janin, J.; Wodak, S.; Levitt, M.; Maigret, B. Conformation of amino-acid side-chains in proteins. *J. Mol. Biol.* **1978**, *125* (3), 357–386.

JP1082467